

**NUMERIC SIMULATION OF ULTRA-HIGH  
PRESSURE ROTARY ATOMIZING WATERJET FLOW FIELD**

Xue Shengxiong, Li Jiangyun<sup>\*</sup>, Peng Haojun, Chen Zhengwen, Wang Yongqiang, Zhu Huaqing  
General Machinery Research Institute  
Hefei, Anhui Province, P. R. China

<sup>\*</sup> Wuhan University, Wuhan, Hubei Province, P. R. China

**ABSTRACT**

Rust dismantling process using ultra-high pressure waterjet is carried out in a close vacuum cavity. When ultra-high pressure water flows out from nozzles, there is a temperature rise of 90°C generated. This temperature rise, combined with the powerful suction force produced by vacuum system and the atomization of waterjet brought by fast rotation of spraying rods, helps to achieve the process's goals, which are cleaning the metal surface to expose its "White Base", drying the cleaned surface just after dismantling and generating no rust in a determined period after treatment. In this paper, the numeric simulation for complicated flow field of multi-bundle ultra-high pressure striking waterjet in a restricted space is conducted with the help of Mixture model for air and fluid two-phase flow, the  $k-\omega$  model for turbulence flow and the FLWEN+ software. The conclusions are: 1) the optimizing range for pressure and speed of flow field is  $S$  (the striking distance from nozzle outlet to cleaning surface) = 7 ~ 15mm; 2) the striking force and shearing force of high-speed waterjet vary with the changing of  $S$ . They reach their peak values when  $S = 15$ mm. This result is also consistent with the test results; and 3) the stability and convergence of  $k-\omega$  model are the best among all applicable simulation models for turbulence flow, these lead to less computational time and higher efficiency.

## 1. INTRODUCTION

Ultra high pressure waterjet technology has been put in wider and wider use in rust dismantling area for its advantages of less environmental pollution, less labor strength and higher automation in operation, etc. To utilize the power of high speed waterjet stream to maximum extent, the characteristics of flow field in vacuum cavity of cleaning robot should be thoroughly investigated.

Four functions and phenomenon in the vacuum cavity of ultra-high pressure waterjet suction rust dismantling robot contribute to the fulfillment of cleaning process, which are: 1) four ultra-high pressure waterjet flow from four eccentrically installed nozzles, and the reaction torque makes the nozzle body rotate, generate the rotating jets and achieve the “White Base” effect during surface preparation on steel surface; 2) the cleaning robot, which is driven by two electric motors, is attached to surface by the suction force produced by the -0.06 MPa vacuum; 3) the cleaned wasted water and debris is sucked away by vacuum suction system during vacuum attaching and dismantling, and the cleaned surface will dry just after dismantling process; 4) the 90°C temperature rise generated after ultra-high pressure water flows out of nozzle hole combined with the vaporization at this temperature helps to achieve the goal of no re-rusting for 15 hours after dismantling with water and providing a good condition for painting. Figure 1. shows the structural diagram of the cleaning robot.

In this paper, the k- $\omega$  model is used to simulate the complex flow field in vacuum cavity, and the results reveal the mechanical characters of the investigated flow field. Tests show that the result of numeric simulation conforms to practice well.

## 2. TURBULENCE MODEL

The average Reynold N-S equation is:

I Continuously equation:

$$\frac{\partial \rho}{\partial t} + \frac{\partial}{\partial x_i} (\rho u_i) = 0$$

II Momentum equation:

$$\frac{\partial}{\partial t} (\rho u_i) + \frac{\partial}{\partial x_j} (\rho u_i u_j) = \frac{\partial p}{\partial x_i} + \frac{\partial}{\partial x_j} \left[ \mu \left( \frac{\partial u_i}{\partial x_j} + \frac{\partial u_j}{\partial x_i} - \frac{2}{3} \delta_{ij} \frac{\partial u_l}{\partial x_l} \right) \right] + \frac{\partial}{\partial x_j} (-\rho \overline{u_i' u_j'})$$

The average Reynold N-S equation is in the same form as its transient form, but the approximate method such as Boussinesq hypothesis that simulates the Reynold stress item of  $-\rho \overline{u_i' u_j'}$  should be applied to make the equation group close. Different assumption will lead to many kinds of turbulence models.

III k- $\omega$  model: k- $\omega$  model is based on turbulence energy equation and diffusion rate equation, and its basic standard form can be shown as:

$$\frac{\partial}{\partial t}(\rho k) + \frac{\partial}{\partial x_i}(\rho k u_i) = \frac{\partial}{\partial x_j}(\Gamma_k \frac{\partial k}{\partial x_j}) + G_k - Y_k + S_k$$

$$\frac{\partial}{\partial t}(\rho \omega) + \frac{\partial}{\partial x_i}(\rho \omega u_i) = \frac{\partial}{\partial x_j}(\Gamma_\omega \frac{\partial \omega}{\partial x_j}) + G_\omega - Y_\omega + S_\omega$$

Where,  $G_k$  — Turbulence kinetic energy generated by laminar flow speed grads;

$G_\omega$  — Generated by  $\omega$  equation;

$T_k, T_\omega$  — k and  $\omega$  diffusion rate correspondingly;

$Y_k, Y_\omega$  — Turbulence generated by diffusion correspondingly;

$S_k, S_\omega$  — Source items defined by calculator.

Diffusion coefficient in k- $\omega$  model are:

$$\Gamma_k = \mu + \frac{\mu_t}{\sigma_k}; \quad \Gamma_\omega = \mu + \frac{\mu_t}{\sigma_\omega}$$

Here,  $\sigma_k, \sigma_\omega$  are the Prandtl Number of turbulence energy in k- $\omega$  equation; and  $\mu_t$  is the turbulence viscosity.

### 3. BOUNDARY CONDITIONS AND MESH DIVISION

#### 3.1 Mesh Division

According to the design request, the inner diameter of cleaner's cavity is  $\varnothing 330\text{mm}$  and the diameter of exhaust tube is  $\varnothing 100\text{mm}$ . Four nozzles are installed symmetrically to the axis of cavity and the distance to shaft center of cavity is 150mm, nozzles extrude 1 mm in the cavity. Since the striking distance is varied, we can fulfill the physics modeling and numeric simulation under three striking distances, which are 200mm, 180mm and 160mm. Because the cavity and exhaust tube can be divided into two symmetrical calculation fields, calculation field is defined as half of the symmetrical cavity for time saving purpose and the triangle meshes are used in calculation of cavity and nozzles. Calculation fields and mesh division are shown in Figure 2.

### **3.2 Boundary Conditions**

Pressure inlet boundary conditions for four nozzles are 200MPa whole pressure, 160MPa static pressure. Pressure outlet boundary condition for exhaust tube is 0.04MPa absolute pressure. For the purpose of studying the heat and mass transfer situation during jet impact, fluid temperatures of 300K and 353K and vapor content of 0.001 and 0.5 are defined as the boundary conditions for inlet and outlet.

## **4. NUMERIC SIMULATION**

### **4.1 Question Prototype and Computational Method**

The moving cleaning request makes design of the total equipment adopt ultra high pressure unit driven by diesel engine as the source of high pressure and powerful waterjet; dismantling work is fulfilled by small diameter plane cleaner with four micro-hole nozzles installed and driven to rotate by jet reaction torque; the plane cleaner is attached to cleaning surface by vacuum suction force generated by vacuum system and the wasted water and cleaned debris are sucked away to achieve the effect of drying just after dismantling. According to this design, assumptions for dismantling impact jet flow field are listed as following:

The high pressure oblique impact jets are simplified to vertical impact jets for ease of calculation considering the declining angles of nozzles are relatively small and the Reynold number reaches up to 120000. That is to say, the oblique impact jet flow field is not within the research scope in this paper.

Nozzles are assumed to extrude into the cavity, and the jet field dose not rotate in cavity. The rotating jet field model is not considered in this paper though actually, the real flows are rotating impact flows revolving along the axis of cavity and propelled by reaction torque generated by slanted four nozzles.

There is no heat exchanging between the fluid in cavity and cavity wall. The working pressure, flow rate, temperature and vapor-bearing rate of nozzles, the pressure, temperature and vapor-bearing rate of suction pipe are given according to test conditions.

Mixture model for gas-liquid two phase flow and  $k-\omega$  turbulence model are used to take numeric simulation, and comparison between RSM Reynold stress model and  $k-\omega$  model is also carried out. Attempt to consider cavitation factor within calculation mixture model is also put forward.

## 4.2 Simulation Aims

Adjust the target distance of two opposite installed nozzles to 4, 10, 20mm separately, simulate the pressure field, speed field, speed vector field, impact surface pressure field and impact surface shear stress field to find out the mechanical characteristic parameters at the same target distance and the changing pattern of mechanical characteristic parameters at different target distance.

## 4.3 Simulation Results

The simulation results are shown in Figure 3.

## 5. SIMULATION ANALYSIS

Numeric simulation and discussion of high pressure impact jet flow field in this paper are mainly focused on the influence of changing striking distance  $S$  on flow field, pressure field and shearing stress of jet impact surface (de-rusting surface).

### 5.1 Change of Pressure and Flow Speed along the Axis of Nozzle

As shown in Figure 3.1~3.3 (a) and (b), jet pressure in nozzle drops from 200MPa at the inlet, and declines much at the place close to nozzle outlet. When it flows out of nozzle, the pressure drops to vacuum pressure and the pressure rise around the striking point because of the resisting of cleaning surface. Because the different distances of four nozzles from suction pipe, the impact pressure of nozzle closest to suction pipe is larger than others for the ambient pressure is lower, and the maximal speed of accelerating zone is larger. This situation is much more obvious when the striking distance  $S$  is 7~15mm, and if  $S$  is 20~25mm the situation will not be so obvious. The conclusion will be opposite to above when  $S$  is small like 4mm should be investigated further.

### 5.2 Changing Characters in Jet Accelerating Zone

Generally, a working pressure of about 200MPa can produce a jet with speed of about 500m/s. But the numeric simulation results show that the jet speed can be accelerated up to 700~800m/s because of the existing vacuum atmosphere in cleaning cavity and vacuum zone around jet produced by the high speed jet itself. If striking distance is just at the end of accelerating zone, the striking force and transformation efficiency from kinetic energy to pressure energy and mechanic energy (shearing force on cleaning surface) will be raised higher so as to raise the dismantling efficiency. As shown in simulation results, the shearing force is highest at striking distance of 15mm. Compare the calculation results, only the work condition of  $S=15$ mm can make the end of acceleration zone reaches working surface. To others with  $S=4$  or 10mm, the jet speed can not

reach its maximal speed because the striking distance is too short and the acceleration zone does not grow up fully; and to others with  $S=20$  or  $25\text{mm}$ , the jet speed will decline before it reached the cleaning surface because the target distance is too large.

### **5.3 Changes of Surface Pressure, Flow and Shearing Force**

As shown in Figure 3.1~3.3(d) and (e), the impact pressure and shearing force on cleaning surface vary along with the change of striking distance. When  $S=4\sim 10\text{mm}$ , impact pressure and shearing force will decline little by little; and when  $H=15\text{mm}$ , impact pressure and shearing force will increase widely; and when  $H=20\text{mm}$ , impact pressure and shearing force will decline with the increase of target distance. All reasons of those have been discussed above. About the changes of surface pressure and flow, shearing force are shown with Figure 3.4~3.6.

### **5.4 Optimization of Ultra-high Pressure Waterjet De-rusting Working Condition**

Good dismantling effect not only is related to maximum shearing force, but also related to the area affected by shearing force. As shown in Figure 3.5 (a) and (b), the speed distribution before jet reaches working surface is impulse curve pattern. This shows that the area affected by shearing force is smaller because of the smaller striking distance ( $S=7$  or  $10\text{mm}$ ), and this is not good to improve dismantling efficiency; On the contrary, as shown in Figure 3.5 (d), the speed distribution area of jet is much more large at larger striking distance ( $S=20\text{mm}$ ), this decreases the kinetic energy peak and leads to a wider distribution area of jet kinetic energy. All these are not good to improve dismantling efficiency too. As shown in Figure 3.5 (c), the jet impact speed distributes much better because the striking distance is just at the end of accelerating zone, and this makes jet impact speed higher than that in other working conditions. So  $S=15\text{mm}$  is the best working condition to waterjet dismantling in this numeric simulation.

### **5.5 Pressure and Flow Distribution in Cavity**

The cleaner cavity is simplified as shown in Figure 2 (a) to find out the whole situation of pressure and flow changes in cavity. Figure 3.1~3.3(f) and (g) list pressure and flow field in cavity and the axial symmetry surface under different working conditions. From these figures, we can find out that the cavity pressure is vacuum under all working conditions, and there is a low-pressure air mass with  $\text{Ø}70\text{mm}$  existing at the place close to suction outlet, and more, an eddy is appeared at the corresponding place. The center of this eddy is the lowest pressure point. It is the eddy and low pressure zone generated by vacuum suction.

## 6. CONCLUSION

- The optimizing range for pressure and speed of flow field is S (the striking distance from nozzle outlet to cleaning surface) =7~15mm;
- The striking force and shearing force of high-speed waterjet vary with the changing of S. They reach their peak values when S=15mm. This result is also consistent with the test results;
- The stability and convergence of k- $\omega$  model are the best among all applicable simulation models for turbulence flow, these lead to less computational time and higher efficiency.

## References

1. Xue Shengxiong, etc. "Research and Test on Mechanism of Ultra High Pressure Waterjet Rust Dismantling", China Mechanical Engineering, Vol. 20, 2004.
2. Xue Shengxiong, etc. "Part Equations on Ultra High Pressure Waterjet Rust Dismantling", Journal on High Pressure Physics, Vol. 3, 2004.
3. Xue Shengxiong, etc. "Practical Usages of Ultra High Pressure Waterjet Technology", China Mechanical Publishing, 1998.
4. University of Michigan, "Surface Preparation & Coating Handbook SSPC", June 1994.
5. R. Schmid, "Ultra High Pressure Waterjetting for Coating Removal", Proceedings of the 10<sup>th</sup> American Waterjet Conference, Houston, U.S.A., 1999, P895~902.
6. T.Kupscznk, etc. "Removal of Non-skid Coatings from Aircraft Decks", Proceedings of the 11<sup>th</sup> American Waterjet Conference, Minneapolis, U.S.A., 2001, P579~588.
7. D. Wright, etc. "A Study of Rotary Jets for Material Removal", Proceedings of the 9<sup>th</sup> American Waterjet Conference, Dearborn, U.S.A., 1997, P525~540.
8. Li Wei, "Combined Finite Element Analysis and Solutions for Viscous Fluid", Science Press, January 2000.
9. Chen Jingren, etc. "Turbulence Models and Their Finite Element Analysis", Shanghai Jiaotong University Press, 1998.
10. R. S. Miller, C. K. Madnia and P. Givi, "Numerical Simulation of Non-circular Jets", Computer & Fluids, Vol. 24(1), 1995, P1~25

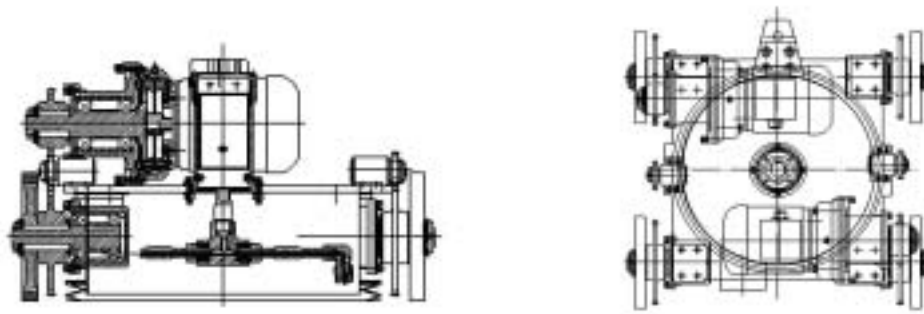
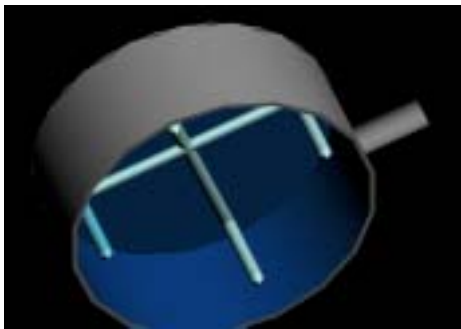
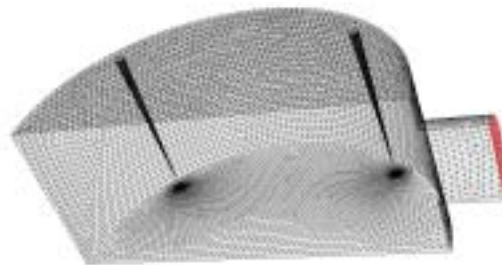


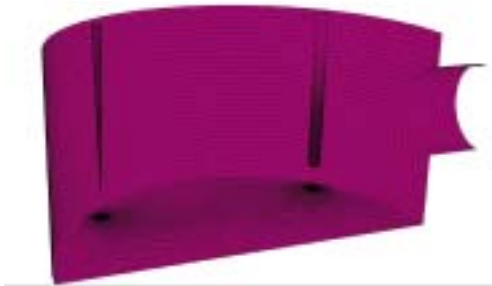
Figure 1 Structural Diagram of Cleaning Robot



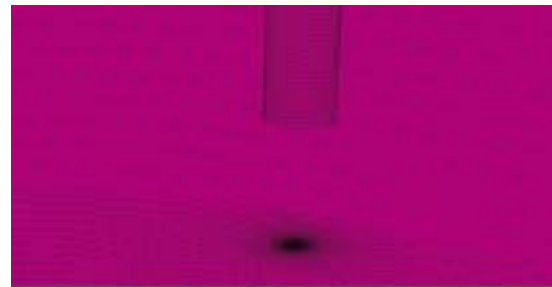
a. Cavity calculation fields



b. Simplified calculation fields

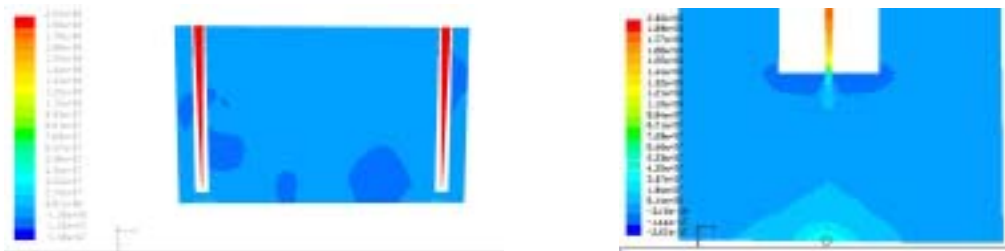


c. Unstructured mesh

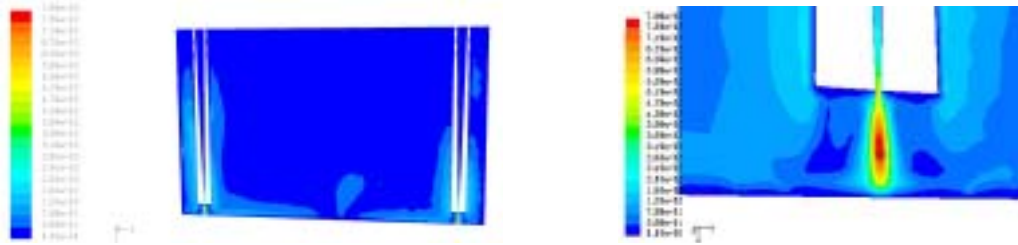


d. Mesh division closed to nozzle

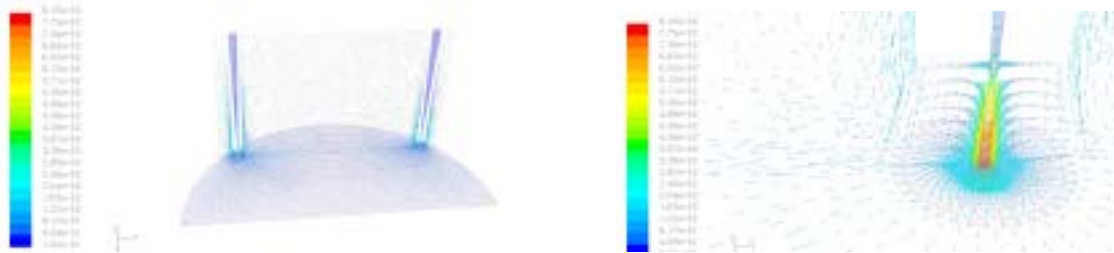
Figure 2 Mesh Division



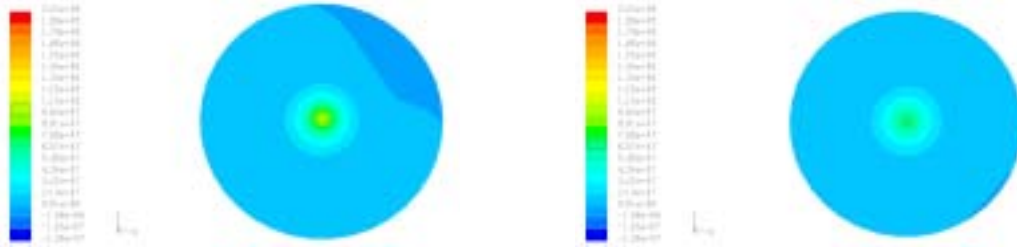
a. High speed jet pressure field



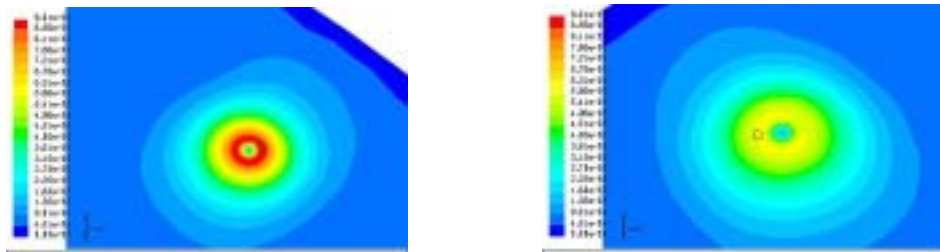
b. High speed jet speed field



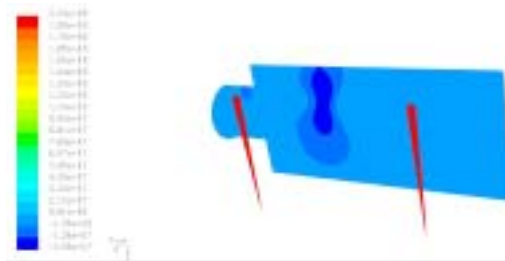
c. High speed jet speed vector field



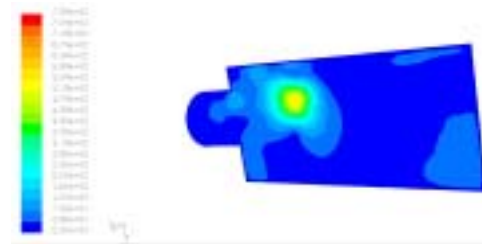
d. Impact surface pressure field



e. Impact surface shearing force field

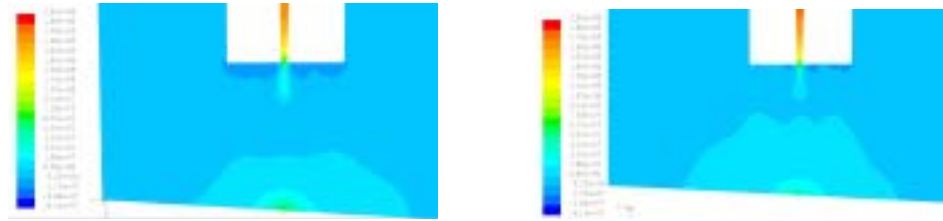


f. Cavity symmetrical plane pressure field

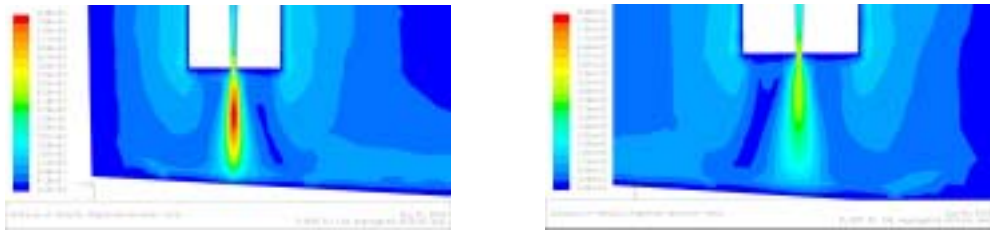


g. Cavity symmetrical plane speed field

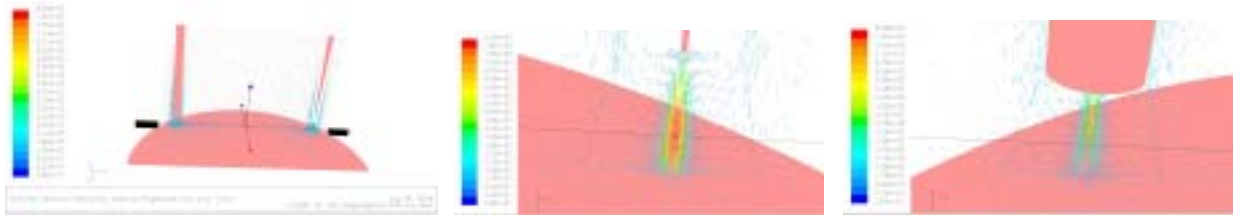
Figure 3.1 Simulation Result with Target Distance  $S=10\text{mm}$



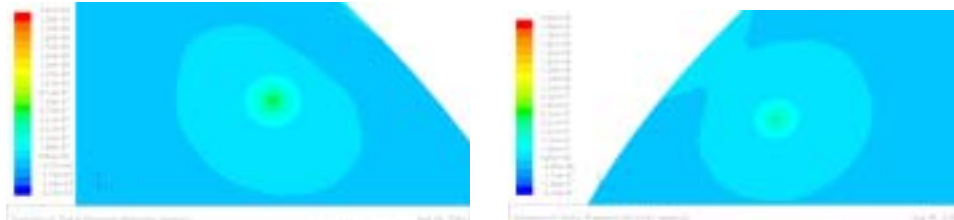
a. High speed jet pressure field



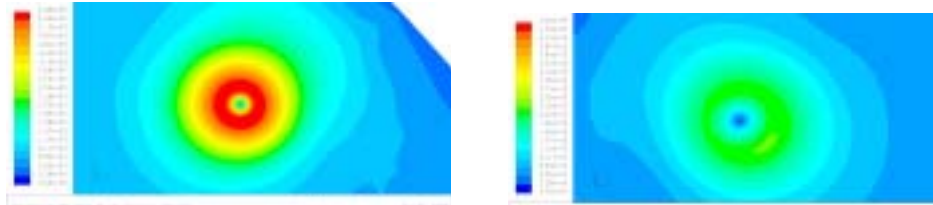
b. High speed jet speed field



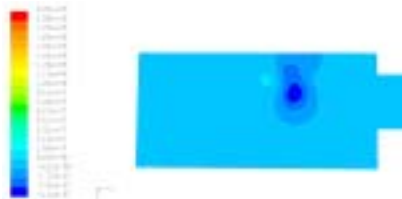
c. High speed jet speed vector field



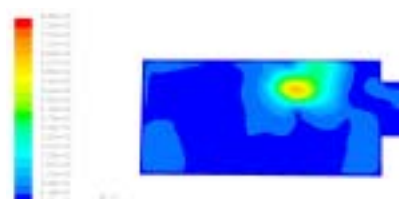
d. Impact surface pressure field



e. Impact shearing force field

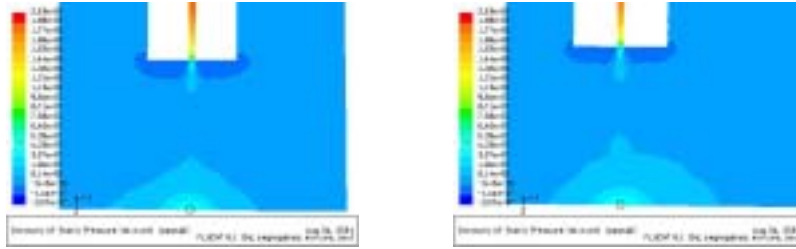


f. Cavity symmetrical plane pressure field

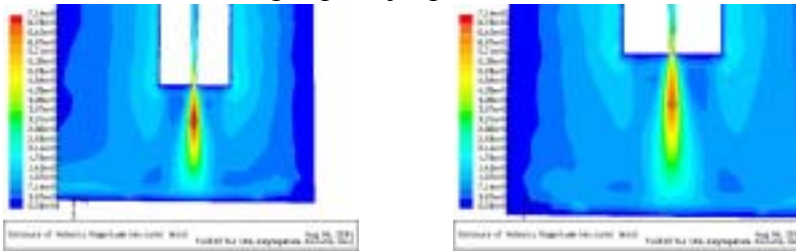


g. Cavity symmetrical plane speed field

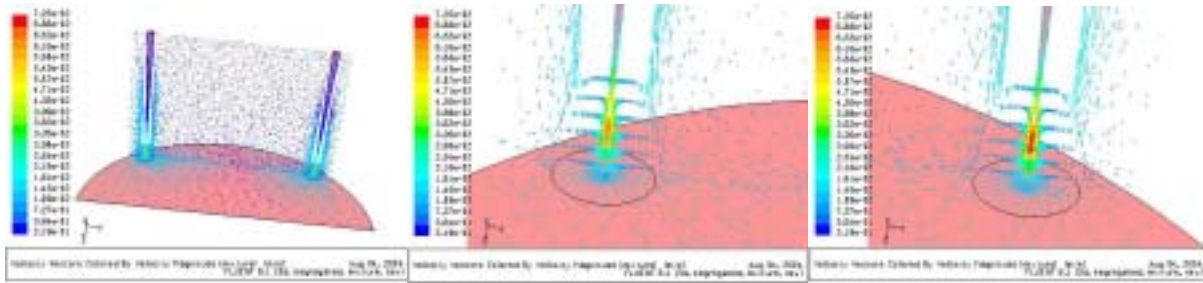
Figure 3.2 Simulation Result with Target Distance  $S=15\text{mm}$



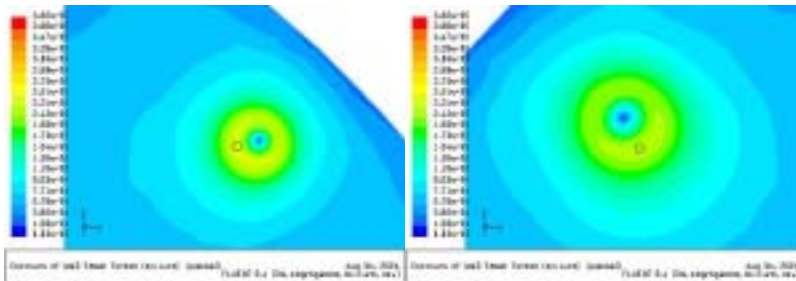
a. High speed jet pressure field



b. High speed jet speed field

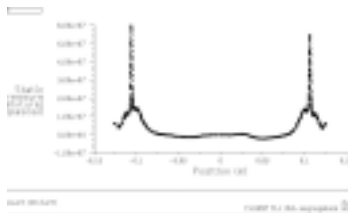


c. High speed jet speed vector field

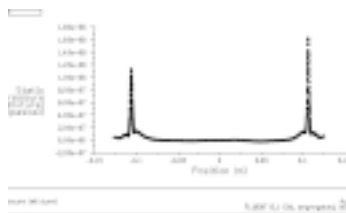


d. Impact shearing force field

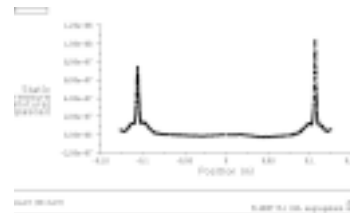
Figure 3.3 Simulation Result with Target Distance  $S=20\text{mm}$



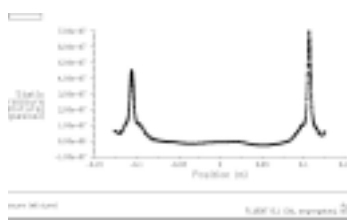
a.  $S=4\text{mm}$



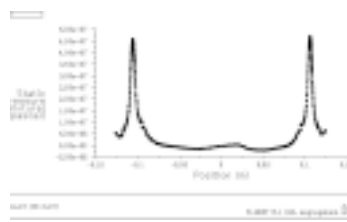
b.  $S=7\text{mm}$



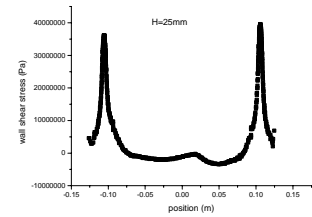
c.  $S=10\text{mm}$



d. S=15mm

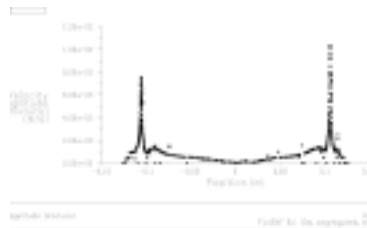


e. S=20mm

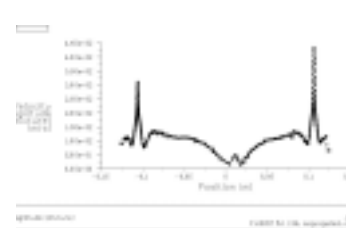


f. S=25mm

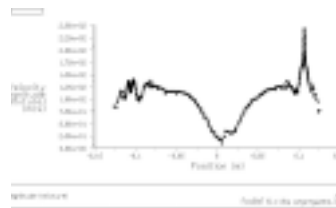
Figure 3.4 Impact force distribution with x=106mm line in the cavity



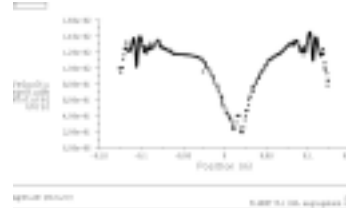
a. S=7mm



b. S=10mm

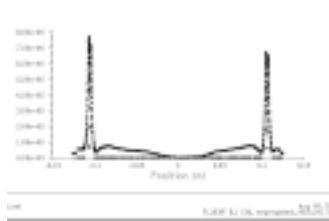


c. S=15mm

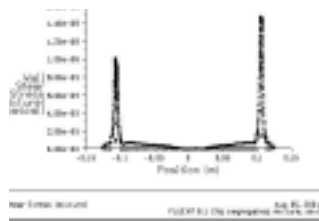


d. S=20mm

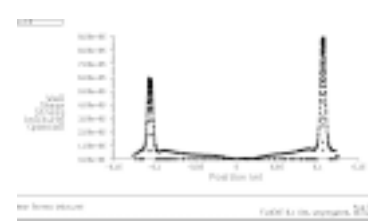
Figure 3.5 Speed Distribution with x=106mm Line in the Cavity



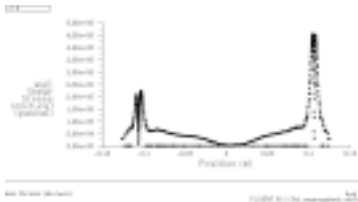
a. S=4mm



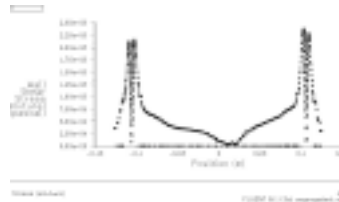
b. S=7mm



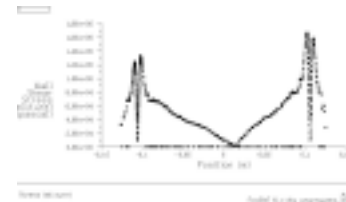
c. S=10mm



d. S=15mm



e. S=20mm



f. S=25mm

Figure 3.6 Shearing Force Distribution with x=106mm Line in the Cavity